New Technique for Synthesizing Concurrent Dual-Band Impedance-Matching Filtering Networks and 0.18-μm SiGe BiCMOS 25.5/37-GHz Concurrent Dual-Band Power Amplifier

Cuong Huynh, *Member, IEEE*, and Cam Nguyen, *Fellow, IEEE*

Abstract—New technique for synthesizing concurrent dual-band impedance-matching filtering networks is presented. The technique enables the design of concurrent dual-band impedance-matching filtering networks that provide not only simultaneous matching of two arbitrary loads to two arbitrary sources at two different frequencies, but also dual-bandpass filtering response capable of suppressing unwanted signals like the harmonics and inter-modulation products in nonlinear circuits, such as power amplifiers (PAs). A new $0.18-\mu$m SiGe BiCMOS concurrent dual-band PA was designed based on the developed dual-band matching filtering technique around 25.5 and 37 GHz, which works in the concurrent dual-band mode (25.5 and 37 GHz), as well as single-band mode (25.5 or 37 GHz). The measured results show that, in the single-band mode, the dual-band PA exhibits gain of 21.4 and 17 dB, maximum output power of 16 and 13 dBm, and maximum power-added efficiency (PAE) of 10.6% and 4.9% at 25.5 and 37 GHz, respectively. In the dual-band mode, the maximum output power is 13 and 9.5 dBm at 25.5 and 37 GHz, respectively, and the total maximum PAE is 7.1%. The designed concurrent dual-band PA has a chip size of 1.3×0.68 mm^2 and consumes a dc current of 120 mA from a 3-V supply voltage.

Index Terms—Dual-band matching, dual-band power amplifier (PA), multiband matching, multiband PA, RF integrated circuit (RFIC).

I. INTRODUCTION

ADVANCED communication and radar systems working "concurrently" over multiple bands provide numerous advantages and have more capabilities as compared to their single-band counterparts for communications and sensing. Achieving concurrent functions over multiple bands enables one single system to be used at multi-band simultaneously, leading to optimum size, cost and power consumption, and ease in realization for the system. True concurrent multiband systems require

many components to work concurrently in multiple bands. Concurrent multiband power amplifiers (PAs) are one of them.

Concurrent multiband PAs that work "only" within the desired bandwidths in multiple bands is attractive. One of the important design criteria for such concurrent multiband PAs, like other concurrent multiband components, is their ability to exhibit concurrent multiband matching. Concurrent multiband matching may be achieved by implementing a filter function separately or internally within a matching network. Combining matching and filtering, particularly with suppression of undesired signals, such as harmonics and inter-modulation products (IMPs), in a single matching network is attractive as it would result in a simple architecture, yet is also very challenging. In the following, we will provide a brief review of nonconcurrent and concurrent multiband PAs and corresponding multiband matching.

Various approaches have been implemented for nonconcurrent multiband PAs operating up to 8 GHz [1]–[5]. In [1] and [2], a quad- and dual-band PA module is formed by combining four and two individual single-band PAs in parallel, respectively. Each individual PA is optimized for a narrowband, and in operation, is selected by switching on the corresponding power supply. This approach, although producing optimum performance in each band, results in large circuit size, and hence, increased cost whereas, more importantly, it can only produce operation in one band at each time, and is thus not suitable for concurrent multiband operation. In [3]–[5], multiband PAs are implemented through reconfiguration of the components in the matching networks. In this approach, the same active devices are used for all bands, while the matching networks are adaptive with the operating bands by reconfiguring the passive components using RF switches or varactors. This approach significantly reduces the number of active devices; hence, the amplifier area and cost, while maintaining optimum performance at all bands. It, however, results in increased circuit complexity due to the use of additional control circuits. Additionally, these multiband PAs can only be operated in a single band at each time instead of in a concurrent multiband.

Several PAs working to 5.2 GHz using concurrent multiband matching networks were reported in [6]–[9]. The performance of these multiband PAs is very much related to the technique used in the design of the matching networks. The dual-band PA in [6] uses a dual-band matching network consisting of two parallel lumped-element resonators on two parallel paths,

each blocking the signal at one frequency. L-type dual-band matching networks consisting of series- and shunt-LC circuits are used in [7]. Dual-band PAs with dual-band matching networks, including harmonic-tuning circuits, using both lump elements and transmission lines are presented in [8] and [9]. The concept of the impedance buffer developed in [8] allows implementation of the multiband harmonic termination by matching the device output with purely imaginary impedances, resulting in improved performance.

Dual-band matching techniques using transmission lines were reported in [10]–[13]. These impedance-matching approaches, although interesting for the design of dual-band components, may not be very suitable for CMOS/BiCMOS implementations since they result in large circuit size, and hence, cost.

The approaches in [6]–[13] mainly focus on dual-band matching techniques; they do not discuss the suppressions of the harmonics and IMPs, which are very crucial for improving the performance of concurrent dual-band PAs.

Advanced SiGe HBTs possess RF performance comparable to III–V compound based HBTs, while having the advantage of compatibility with standard CMOS technologies, which results in increased integration capability and low cost [14]. Many CMOS and SiGe HBT PAs have been designed at K- and Ka-bands [15]–[19]. All of them, however, are single-band PAs. To date, there has been no concurrent dual-band PA operating at K/Ka-band or, as a matter of fact, above 5.2 GHz reported.

The objective of this paper is twofold. First, it presents a new design methodology for concurrent dual-band impedance-matching filtering networks. This design method, while suitable for both lumped elements and transmission lines, is specifically formulated using lumped elements for possible on-chip implementations for miniature RF integrated circuits (RFICs), particularly on CMOS/BiCMOS processes. Various concurrent dual-band matching filtering networks can be synthesized using the proposed technique, which not only enable simultaneous matching of two arbitrary loads to two arbitrary source impedances at two arbitrarily different frequencies, but also suppress unwanted signals, such as harmonics and IMPs in nonlinear circuits. The suppression of harmonics and IMPs is especially crucial for PA design in particular and other nonlinear circuits in general, yet has not been discussed in any dual-band PA papers published to date. It should be noted that, although the dual-band filtering characteristics are reported in other dual-band PA papers, having a dual-band filtering response does not mean that the amplifiers have the ability to suppress the harmonics and IMPs. A dual-band PA with a filtering function can produce the dual-band filtering response for the gain, but it cannot suppress the harmonics and IMPs if these signals are not incorporated in the design. On the other hand, if the harmonic and IMP suppressions are considered in the amplifier design as presented in this paper, a dual-band filtering response becomes inherent.

Second, the paper reports for the first time a dual-band PA working concurrently at 25.5 and 37 GHz designed using the developed concurrent dual-band matching technique. Important design issues for concurrent dual-band PAs and detailed design of the 25.5/37 GHz PA are also presented. The designed

dual-band PA exhibits measured gains of 21.4 and 17 dB at 25.5 and 37 GHz, respectively, in both single- and concurrent dual-band modes. It also has maximum measured output powers of 16/13 and 13/9.5 dBm at 25.5/37 GHz in the single- and concurrent dual-band mode, respectively. The PA has a chip size of 1.3×0.68 mm^2 and consumes a dc current of 120 mA from a 3-V source.

II. METHOD FOR SYNTHETIC CONCURRENT DUAL-BAND IMPEDANCE-MATCHING NETWORKS

Concurrent dual-band impedance-matching networks are required to match two different impedances (herein referred to as load impedances) to two other different impedances (referred to as source impedances) at two different frequencies. A matching network is typically used to provide matching at a single band, which is implemented in conventional single-band designs. We can infer in theory that, in order to provide concurrent matching over dual-band (or, in general, multi-band), two single-band (or multiple single-band) matching networks would be needed. Using two separate matching networks to achieve dual-band matching, however, is not effective. A logical question is then: can a single network be synthesized from two different single-band matching networks to achieve concurrent matching at two different bands? To answer this question, we first consider general single-band lumped-element matching networks consisting of inductors and capacitors. Second, we recognize that any LC network can be equivalent to an inductor, capacitor, open, or short at different frequencies. This leads to the possibility that an LC network can be used to realize inductor, capacitor, open, or short at different frequencies simultaneously. We can then conclude that it is possible to combine two separate single-band matching networks at two different frequencies into a single network that provides concurrent matching at these frequencies. Our proposed dual-band matching filtering technique and the resultant networks, hereafter referred to as "synthetic concurrent dual-band matching networks," are derived based on this basic idea. It is particularly noted that the short- and open-circuited characteristics at certain frequencies of the LC networks used in the dual-band matching also result in the suppression of unwanted signals such as harmonics and/or IMPs, which are useful for the design of nonlinear components such as PA.

The key of our proposed concurrent dual-band matching design is based on LC networks that can function as an inductor, capacitor, open, or short at different frequencies simultaneously. Table A1 contains some possible LC networks that can be used to synthesize concurrent dual-band matching filtering networks. It is noted that our proposed approach is not limited to the LC networks in Table A1 other LC networks can also be used. Any LC network in Table A1 can be used to exhibit not only its equivalent inductance or capacitance at certain frequencies for the design of concurrent dual-band matching networks, but also open and/or short at other frequencies such as harmonics or IMPs for signal suppression. For instance, Network 6 behaves as an inductor at $\omega < \omega_{02}$ or $\omega > \omega_{01}$, a capacitor at $\omega_{02} < \omega < \omega_{01}$, open at $\omega = \omega_{02}$, and short at $\omega = \omega_{01}$. When used in shunt, Network 6 suppresses signals at $\omega = \omega_{02}$, whereas it blocks signals at $\omega = \omega_{02}$ when connected in series. It is particularly noted that the LC networks listed in Table A1
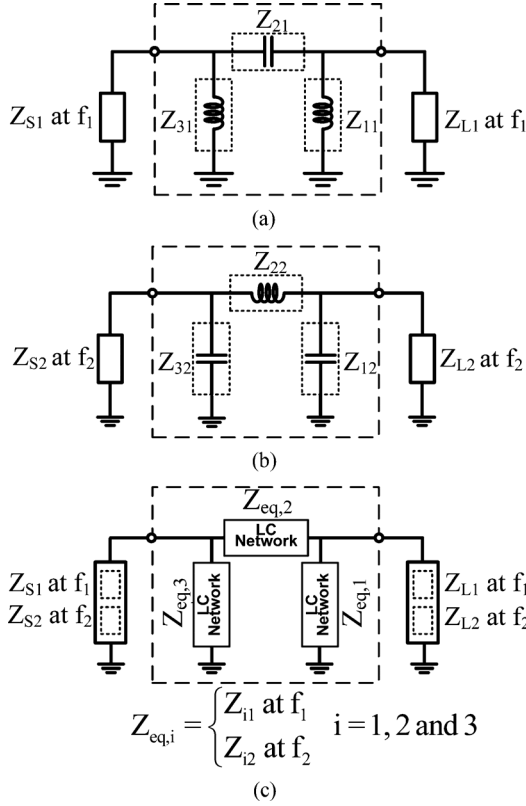
Fig. 1. Single-band matching network at: (a) $f1$ and (b) $f2$, and (c) synthetic dual-band matching network.

are not dual band and they can be found in standard network and microwave engineering books. However, to the best of our knowledge, the method to properly combine them to synthesize dual-band matching filtering networks that can perform concurrent dual-band functions together with suppression of unwanted signals like the harmonics and IMPs has not been reported.

The proposed matching-filtering synthesis method that allows many possibly new dual-band matching networks with unwanted-signal suppression characteristics to be systematically designed is now described. Fig. 1 illustrates the design process for a concurrent dual-band matching filtering network to simultaneously transfer Z_{L1} to Z_{S1} and Z_{L2} to Z_{S2} at f_1 and $f_2 (f_1 < f_2)$, respectively. It consists of the following three steps:

First, two separate single-band lumped-element matching networks transforming Z_{L1} to Z_{S1} at f_1 and Z_{L2} to Z_{S2} at f_2 are designed using a suitable matching technique (e.g., [20]) as shown in Fig. 1(a) and (b). In each branch of the single-band matching networks, there is at most one inductor or one capacitor having impedance/admittance of Z_{i1}/Y_{i1} at f_1 and Z_{i2}/Y_{i2} at f_2, $(i = 1, 2, 3)$. It is noted that the corresponding components in the two single-band matching networks do not need to be dual of each other. The two single-band matching networks can be different and of any type, such as L-type or Pi-type, having two or more elements, and the number of elements in each matching network does not need to be the same. The Pi-type matching networks are used in Fig. 1(a) and (b) to signify the generality of the proposed dual-band matching filtering technique.

Second, a dual-band matching network is synthesized from the two designed single-band matching networks. This is done by replacing every two corresponding branches of the two single-band matching networks with an appropriate LC network such as that from Table A1 having its equivalent impedance of $Z_{eq,i}$ satisfying

$$Z_{eq,i} = Z_{i1}, \qquad \text{at } f = f_1 \qquad (1)$$
$$Z_{eq,i} = Z_{i2}, \qquad \text{at } f = f_2 \qquad (2)$$

as shown in Fig. 1(c). The dual-band matching network is electrically equivalent to the two single-band matching networks working simultaneously at two frequencies f_1 and f_2. It is noted that admittances $Y_{eq,i}$, Y_{i1}, and Y_{i2} can also be used in lieu of impedances.

Third, the two equations resulting from conditions (1) and (2) are solved for each LC network to determine L's and C's. It is noted that the two conditions in (1) and (2) are only sufficient for two-element LC networks such as Network 1 and 2 in Table A1. For other LC networks having more than two elements, other specific conditions required for the design need to be used—for instance, the harmonic/IMP suppression condition, in which the LC network becomes an open or short at the harmonic/IMP frequency, which is used for the design of the dual-band PA in Section III. Conditions (1) and (2), and other possible conditions, produce a simple set of two-variable linear equations that are easy to be solved. It is noted that, for certain cases, real values for L and C may not be obtained and, in these cases, other conditions or even other LC networks need to be used instead. By properly choosing LC networks, a resultant synthetic concurrent dual-band matching filtering network can exhibit not only dual-band matching, but also dual-band filtering and harmonic/IMP suppression.

A synthetic dual-band matching network inevitably requires more LC elements than a single-band matching network; hence, reducing the overall quality factor and increasing the loss of the matching network. Therefore, it is important to choose proper constituent LC networks—for instance, those having less elements—and improve the quality factor of on-chip inductors to minimize the loss for the dual-band matching networks. Similar formulation can be used to derive synthetic concurrent dual-band matching networks consisting of only transmission lines or combined lumped elements and transmission lines. Specifically, for concurrent dual-band matching networks of transmission lines, two separate single-band transmission-line matching networks would need to be designed first. A dual-band matching network is then synthesized from these single-band matching networks using appropriate transmission-line networks. Moreover, conditions such as (1) and (2), as well as other conditions such as the harmonic/IMP suppression condition are also utilized in the design. The design of concurrent dual-band transmission-line matching networks, however, is more involved and requires development of various transmission-line networks to be used for the synthesis. Detailed implementation of the proposed dual-band matching filtering technique for the design of the output, inter-stage, and input dual-band lumped-element matching networks of the 25.5/37-GHz dual-band PA is described in Section III.
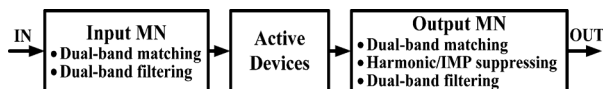
Fig. 2. Main blocks of a concurrent dual-band PA.

Fig. 3. Output spectrum of the designed PA (without the output matching network) with two concurrent input tones at 25.5 and 37 GHz.

Lastly, it is particularly remarked that the closeness of the dual bands to each other depends on the ability of an LC network to represent an element (inductor or capacitor) at f_1 and another element (inductor or capacitor) at f_2 at the same time. As there are many possible LC networks that can be used in the proposed method, this implies that a sole analysis describing the proximity of the dual bands for all possible LC networks is not possible. This property should be considered for each particular LC network used in the method. This matter is further complicated by the fact that our proposed method also considers the suppressions of unwanted harmonics and IMPs. The most effective way, as far as design is concerned, is to conduct a numerical analysis for a chosen LC network to study how close the dual bands can be, and if it does not meet the requirement, then use different LC networks accordingly. This can be done relatively easy during the design process.

III. 5/37-GHz CONCURRENT DUAL-BAND PA

The 25.5/37-GHz concurrent dual-band PA was designed utilizing the proposed concurrent dual-band matching filtering technique and fabricated using Jazz $0.18 - \mu$m SiGe BiCMOS process.[1] The SiGe HBT transistors used for the PA have breakdown voltages $\mathrm{BV_{CEO}} = 1.9$ V and $\mathrm{BV_{CBO}} = 5.8$ V. The topmost metal layer is used for the inductors, ac ground, and interconnects. All the on-chip inductors, interconnects, vias and ac ground were designed and simulated using the electromagnetic (EM) simulator IE3D. The PA was simulated, optimized, and laid out using Cadence. All combining networks connecting HBT's base, emitter, and collector terminals were carefully simulated using IE3D before running the load–pull simulation.

A. Concurrent Dual-Band PA Design Issues

Fig. 2 shows the building blocks with their essential functions of a concurrent dual-band PA. Dual-band inter-stage matching networks are also needed for multi-stage dual-band PAs. The active-device block may consist of one or several transistors.

The design of the input and output matching networks of a concurrent dual-band PA is much more challenging than that of a single-band PA. In a single-band PA, the input and output matching networks provide matching only at one fundamental frequency to attain highest possible performance such as maximum output power or power-added efficiency (PAE). In addition, the single-band output matching network also needs to include harmonic control circuits to improve the PA performance [21]. In a concurrent dual-band PA, the PA is operated under dual mode and is subjected to two-tone large-signal conditions. The active devices thus generate many more unwanted harmonics and IMPs than a single-band PA, which need to be
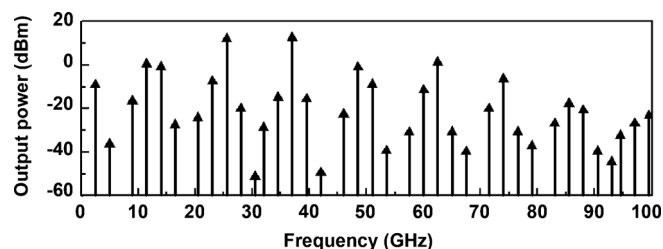
suppressed for achieving good PA performance and avoiding harm to other components and systems. To illustrate this possible complex spectrum, we show in Fig. 3 the output spectrum of the designed PA (without the output matching network) that is simultaneously fed with two tones at 25.5 and 37 GHz. It is observed that, besides the two fundamental tones, there are many harmonics and IMPs generated due to the inherent nonlinearity of the active devices. While the harmonics of the two tones are located at their upper side, the IMPs are distributed below, between, and above the two fundamental frequencies. To achieve the best possible performance for a concurrent dual-band PA, the output matching network is required to not only match the 50-Ω load to optimum output impedances at two different fundamental frequencies, but also to suppress the harmonics and IMPs. It is apparent that suppressing the IMPs located very close to the two main tones is rather challenging, as this requires very high-Q networks, which are difficult to achieve at millimeter-wave frequencies. Moreover, the bandwidth of the concurrent dual-band PAs designed using the proposed dual-band matching approach is expected to be smaller than that of their single-band counterparts in order to sufficiently suppress these IMPs. Like the output matching network, the input matching network is required to simultaneously match the source with optimum input impedances at two different frequencies. The inter-stage matching networks, needed in multi-stage PAs, are required to match two different input impedances of the next stage to two different optimum output impedances of the previous stage at two different frequencies, as well as suppress unwanted harmonics and/or IMPs generated from the previous stage. In addition to concurrently matching in dual band, all the input, inter-stage, and output matching networks should have a dual-band filtering response to reduce the interferences generated by the PA to the existing components and systems, and reject the out-of-band signals possibly injecting into the PA and desensitizing the two main tones.

Techniques for impedance matching at one frequency, such as that described in [20], is relatively straightforward and widely used. However, simultaneously matching two arbitrary loads to two arbitrary source impedances at two different frequencies using lumped components required for concurrent dual-band matching networks, along with the suppression of undesired signals like harmonics and IMPs needed for nonlinear components such as dual-band PAs, is still a challenging issue. This can be addressed using the proposed concurrent dual-band matching filtering design technique described in Section II, as implemented for the 25.5/37-GHz PA design reported here.

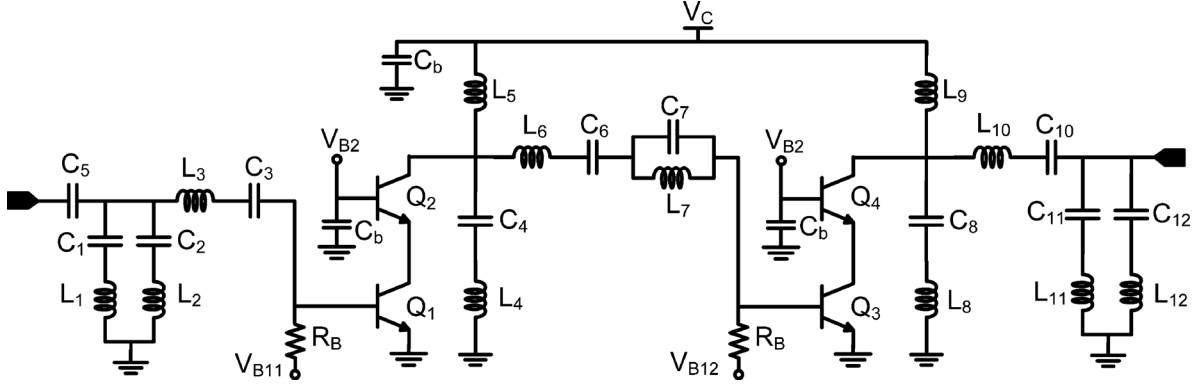[1]TowerJazz Semiconductor, Newport Beach, CA, USA.

Fig. 4. Schematic of the 25.5/37-GHz concurrent dual-band PA.

B. PA Circuit, Device, and Bias

Fig. 4 shows the schematic of the designed 25.5/37-GHz concurrent dual-band PA that consists of two cascode stages and three dual-band matching networks including input, inter-stage, and output matching networks. The dual-band PA is biased to work in the class-AB mode. The cascode PA topology allows the transistor to operate at a voltage higher than the breakdown voltage and provides maximizing gain and output power simultaneously [18], [22]. In the cascode pairs, the common-emitter transistors determine the gain for the PA while the common-base transistors with possibly high power supply voltage enable high RF output power [22]. In addition, the cascode structure provides high reverse isolation between the input and output; hence, increasing the stability for the PA at high frequencies.

High-performance SiGe transistors used in this design suffer the problem of low breakdown voltage of $B_{\text{VCEO}} = 1.9$ V. It has been shown that the common-emitter transistor with small base resistor can work at the collector–emitter voltage much higher than the base-open breakdown voltage BV_{CEO}[22], [23]. Thus, the bases of transistors Q_1 and Q_3 are biased through resistors of 300 Ω to allow them to work at an increased voltage swing. The base voltage of Q_2 and Q_4 are set at 1.8 V to keep transistors Q_1 and Q_3 working in the forward-active region and minimize the knee voltage for the cascode pair; hence, maximizing the dynamic output voltage swing [23]. The bias voltage at the collectors of transistors Q_2 and Q_4 is of more concern for high-power cascode PAs. It needs to be high for high RF output power, but must be within a constraint to keep these transistors away from breakdown. The experimental study in [23] recommends that the maximum collector bias voltage V_C for maximizing the power performance and dynamic safe-operation area for cascode PAs to be lower than $1/2(\text{BV}_{\text{CBO}} + V_{B\_Q2} + V_{\text{knee}})$, which is 4.3 V for the SiGe HBT used in the designed dual-band PA, where V_{knee} is around 1 V obtained from the simulated dc characteristic of the cascode pair. This ensures that the PA will undergo a gain compression before breakdown. The designed dual-band PA is biased at collector voltage V_C of 3 V.

Increased RF output power can be achieved by connecting many SiGe HBTs in parallel, necessitating the use of wide metal trips for interconnects and inductors to meet the required current density. However, using wide metal traces for inductors introduces more parasitic capacitances, which affect the PA per-

formance, especially at high frequencies. The number of parallel transistors used in a cascode stage is, hence, limited. In the designed dual-band PA, the common-emitter transistor Q_3 and common-base transistor Q_4 in the last cascode stage is each constituted from four parallel transistors, while the common-emitter transistor Q_1 and common-base transistor Q_2 in the first stage each consists of two transistors. Each transistor has an emitter area of 0.15×20.32 μm^2 with two emitter, three base, and two collector contacts. All transistors are biased at a current density of 10 m A$/\mu\text{m}^2$ for maximum f_{max} of 180 GHz.

The last stage is designed to give highest power efficiency while the first stage is designed to provide maximum output power. Load–pull simulations are used to find the optimum loads at two different frequencies for each stage.

C. Concurrent Dual-Band Output Matching Network Design

The dual-band output matching network is designed to concurrently transfer a 50-Ω load to two optimum impedances $Z_{\text{op1}} = 14.5 + \text{j}7$ Ω and $Z_{\text{op2}} = 12 + \text{j}2$ Ω at $f_1 = 25.5$ and $f_2 = 37$ GHz, respectively, for maximum efficiency, and suppress the harmonics and IMPs. Following the dual-band matching methodology outlined in Section II, two single-band output matching networks are first designed to transfer the 50-Ω load to Z_{op1} and Z_{op2} at 25.5 and 37 GHz, respectively. The 25.5-GHz matching network, as shown in Fig. 5(a), consists of L_{o1}, C_{o2}, and L_{o3}, and the 37-GHz matching network, as shown in Fig. 5(b) consists of C_{o1} and L_{o2}. The concurrent dual-band output matching network, as shown in Fig. 5(c), is synthesized from the 25.5- and 37-GHz matching networks to provide simultaneous output matching at 25.5 and 37 GHz. It consists of Network 6 (C_8, L_8, and L_9), Network 1 (L_{10} and C_{10})), and Network 9 (L_{11}, C_{11}, L_{12}, and C_{12}) from Table A1. These *LC* network types are chosen to not only synthesize the corresponding inductor and capacitor at different frequencies, but also provide short or open at some particular frequencies to suppress the harmonics and IMPs.

1) C_8, L_8, and L_9 (Network 6): Network 6 consisting of C_8, L_8, and L_9 is used to simultaneously synthesize the inductor L_{o3} in Fig. 5(a) at $f_1 = 25.5$ GHz and the corresponding open circuit at $f_2 = 37 hbox{GHz}$ in Fig. 5(b). In addition, this network becomes a short circuit at 52.3 GHz to suppress the harmonic and IMP shown in Fig. 3. The short-circuit frequency
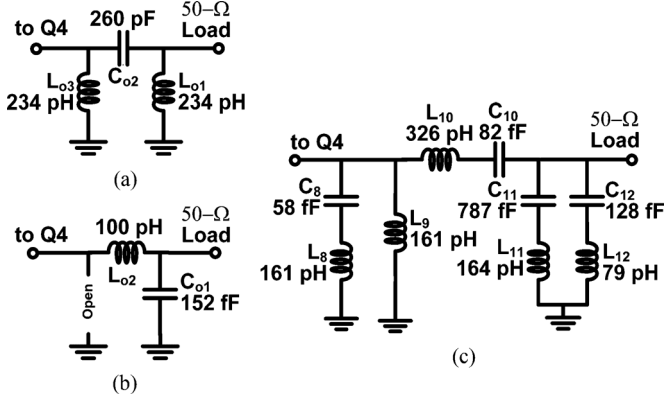
Fig. 5. (a) 25.5- and (b) 37-GHz single-band output matching networks and (c) 25.5/37-GHz dual-band output matching network. An open is included in (b) to make the topologies in (a) and (b) compatible.

of 52.3 GHz is chosen based on the distribution of the harmonics/IMPs in Fig. 3 and to minimize the values of inductors L_8 and L_9; hence, reducing the loss of the output matching network. Moreover, as shown in Fig. 4 the inductor L_9 conducts dc current to bias the cascade pair Q3 and Q4, thus avoiding the use of a bulky RF choke inductor. Making use of the Network-6 admittance expression listed in Table A1, (1) and (2) become

$$\frac{\omega_1 \omega_{01}^2 C_8}{\omega_{01}^2 - \omega_1^2} - \frac{1}{\omega_1 L_9} = -\frac{1}{\omega_1 L_{o3}} \tag{3}$$

$$\frac{\omega_2 \omega_{01}^2 C_8}{\omega_{01}^2 - \omega_2^2} - \frac{1}{\omega_2 L_9} = 0 \tag{4}$$

where $\omega_1 = 2\pi f_1$ and $\omega_2 = 2\pi f_2$. The short-circuit condition is used at

$$\omega_{01} = \frac{1}{\sqrt{L_8 C_8}} = 2\pi \times 52.3 \times 10^9. \tag{5}$$

Equations (3)–(5) can be expressed in a simple set of two-variable linear equations

$$AC_8 + B\frac{1}{L_9} = M \tag{6}$$

$$CC_8 + D\frac{1}{L_9} = N \tag{7}$$

where

$$A = \frac{\omega_1 \omega_{01}^2}{\omega_{01}^2 - \omega_1^2}$$

$$B = -\frac{1}{\omega_1}$$

$$C = \frac{\omega_2 \omega_{01}^2}{\omega_{01}^2 - \omega_2^2}$$

$$D = -\frac{1}{\omega_2}$$

$$M = -\frac{1}{\omega_1 L_{o3}}$$

$$N = 0$$

which are then solved to give the values for L_9, C_8, and L_8 as

$$L_9 = \frac{(AD - BC)}{(AN - CM)} \quad C_8 = \frac{(DM - BN)}{(AD - BC)} \quad L_8 = \frac{1}{C_8 \omega_{01}^2}$$

or $C_8 = 58 hbox fF$ and $L_8 = L_9 = 161$ pH.

2) L_{10} and C_{10} (Network 1): Network 1 consisting of L_{10} and C_{10} is used to synthesize the capacitor C_{o2} in Fig. 5(a) at $f_1 = 25.5$ GHz and inductor L_{o2} in Fig. 5(b) at $f_2 = 37$ GHz. The capacitor C_{10} also functions as a dc block capacitor to prevent dc current from V_{CC} going to the 50-Ω load. Network 1 has less components than other networks; hence, reducing the loss for the output matching network. Using the impedance expression for Network 1 shown in Table A1, we can write from (1) and (2),

$$\omega_1 L_{10} - \frac{1}{\omega_1 C_{10}} = \frac{-1}{\omega_1 C_{o2}} \tag{8}$$

$$\omega_2 L_{10} - \frac{1}{\omega_2 C_{10}} = \omega_2 L_{o2}. \tag{9}$$

Solving (8) and (9) results in

$$L_{10} = \frac{(DM - BN)}{(AD - BC)} \text{ and } C_{10} = \frac{(AD - BC)}{(AN - CM)}$$

where

$$A = \omega_1$$

$$B = -\frac{1}{\omega_1}$$

$$C = \omega_2$$

$$D = -\frac{1}{\omega_2}$$

$$M = -\frac{1}{\omega_1 C_{o2}}$$

$$N = \omega_2 L_{o2}$$

or $L_{10} = 326$ pH and $C_{10} = 82$ fF.

3) $L_{11}, C_{11}, L_{12},$ and C_{12} (Network 9): Network 9 consisting of C_{11}, L_{11}, C_{12}, and L_{12} is used to synthesize the inductor L_{o1} in Fig. 5(a) at $f_1 = 25.5$ GHz and C_{o1} in Fig. 5(b) at $f_2 = 37$ GHz. It also functions as a short circuit at 14 and 50 GHz to suppress the IMPs around 14 and 50 GHz, and the second harmonic of 25.5 GHz near 50 GHz. Equations (1) and (2) become, making use of Network 9's admittance expression,

$$\frac{\omega_1 \omega_{01}^2 C_{11}}{\omega_{01}^2 - \omega_1^2} + \frac{\omega_1 \omega_{02}^2 C_{12}}{\omega_{02}^2 - \omega_1^2} = -\frac{1}{\omega_1 L_{o1}} \tag{10}$$

$$\frac{\omega_2 \omega_{01}^2 C_{11}}{\omega_{01}^2 - \omega_2^2} + \frac{\omega_2 \omega_{02}^2 C_{12}}{\omega_{02}^2 - \omega_2^2} = \omega_2 C_{o1}. \tag{11}$$

The harmonic and IMP suppression conditions are at

$$\omega_{01} = \frac{1}{\sqrt{L_{11} C_{11}}} = 2\pi \times 14 \times 10^9$$

$$\omega_{02} = \frac{1}{\sqrt{L_{12} C_{12}}} = 2\pi \times 52 \times 10^9. \tag{12}$$

Equations (10)–(12) can be rearranged into a set of two-variable linear equations from which C_{11}, L_{11}, C_{12}, and L_{12} can be determined as

$$C_{11} = \frac{(DM - BN)}{(AD - BC)}$$

$$L_{11} = \frac{1}{C_{11} \omega_{01}^2}$$

$$C_{12} = \frac{(AN - CM)}{(AD - BC)}$$

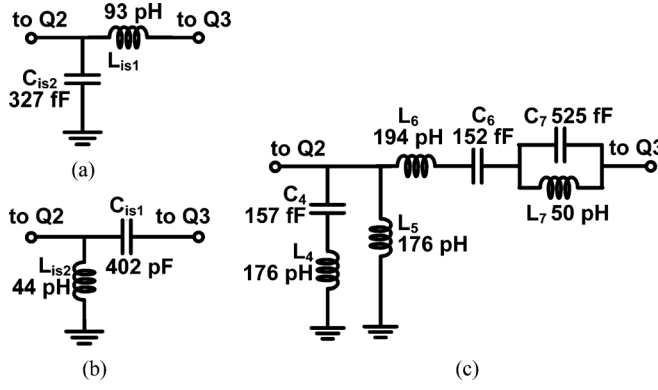$$L_{12} = \frac{1}{C_{12} \omega_{02}^2}$$

Fig. 6. (a) 25.5- and (b) 37-GHz single-band inter-stage matching networks and (c) 25.5/37-GHz dual-band inter-stage matching network.

Fig. 7. (a) 25.5- and (b) 37-GHz single-band input matching networks and (c) 25.5/37-GHz dual-band input matching network.

where

$$A = \frac{\omega_1 \omega_{01}^2}{\omega_{01}^2 - \omega_1^2}$$

$$B = \frac{\omega_1 \omega_{02}^2}{\omega_{02}^2 - \omega_1^2}$$

$$C = \frac{\omega_2 \omega_{01}^2}{\omega_{01}^2 - \omega_2^2}$$

$$D = \frac{\omega_2 \omega_{02}^2}{\omega_{02}^2 - \omega_2^2}$$

$$M = -\frac{1}{\omega_1 L_{o1}}$$

$$N = \omega_2 C_{o1}$$

or $C_{11} = 787$ fF, $L_{11} = 164$ pH, $C_{12} = 128$ fF, and $L_{12} = 79$ pH.

D. Inter-Stage Matching Network Design

The dual-band inter-stage matching network is designed to concurrently match the second-stage's input impedances of $4 - j1.4\ \Omega$ and $4.5 + j1.8\ \Omega$ to the first-stage's output impedances of $30.8 - j24\ \Omega$ and $20.9 - j3.1\ \Omega$ at $f_1 = 25.5$ and $f_2 = 37$ GHz , respectively, maximize the first-stage's output powers at these frequencies, and suppress the IMPs existing at frequencies between the two fundamental tones. The 25.5-GHz single-band inter-stage matching network shown in Fig. 6(a) consists of L_{is1} and C_{is2}, and the 37-GHz single-band inter-stage matching network shown in Fig. 6(b) consists of C_{is1} and L_{is2}. The synthetic dual-band inter-stage matching network consists of Network 6 (C_4, L_4, and L_5) and Network 5 (L_6, C_6, L_7, and C_7). These networks are chosen to not only synthesize the corresponding inductor and capacitor at different frequencies, but also provide short and open at 30.2 and 31 GHz, respectively; hence, suppressing the IMPs existing between the two main tones.

1) L_4, C_4 and L_5 (Network 6): Network 6 consisting of L_4, C_4, and L_5 is used to synthesize the capacitor C_{is2} at $f_1 = 25.5$ GHz and inductor L_{is2} at $f_2 = 37$ GHz. This network also produces a short at $f_{01} = 30.2$ GHz to suppress the IMP existing between f_1 and f_2 and create a dual-band response for the gain. Inductor L_5 conducts dc current to bias the cascade pair Q_1 and Q_2; hence, eliminating the use of a bulky RF choke inductor. The values for C_4, L_4, and L_5 are obtained by solving
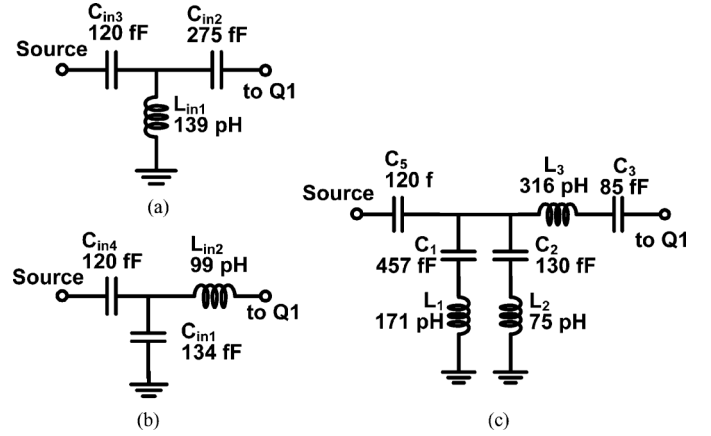
(1) and (2), applying the admittance expression and short-circuit condition for Network 6, resulting in $C_4 = 157$ fF and $L_4 = L_5 = 176$ pH.

2) L_6, C_6, L_7, and C_7 (Network 5): Network 5 consisting of L_6, C_6, L_7, and C_7 is used to synthesize the inductor L_{is1} at $f_1 = 25.5$ GHz and the capacitor C_{is1} at $f_2 = 37$ GHz, while becoming an open circuit at 31 GHz to block the IMP existing between f_1 and f_2 and create a dual-band filtering response. Capacitor C_6 functions as an inter-stage dc blocking capacitor and the open-circuit frequency is determined by the parallel resonator of L_7 and C_7. Applying the impedance expression of Network 5 for (1) and (2), as well as Network 5's open-circuit condition shown in Table A1, we can obtain $C_6 = 152$ fF, $L_6 = 194$ pH, $L_7 = 50$ pH, and $C_7 = 525$ fF.

E. Input Matching Network Design

The dual-band input matching network is designed to concurrently match the first stage's input impedances of $7.4 - j4\ \Omega$ and $7.1 - j0.7\ \Omega$ to the 50-Ω source at 25.5 and 37 GHz, respectively, for maximum gain and reject the out-of-band signals.

Two single-band input matching networks at 25.5 and 37 GHz are shown in Fig. 7(a) and (b), respectively. The first one consists of L_{in1}, C_{in2}, and C_{in3} while the second one consists of C_{in1}, L_{in2}, and C_{in4}. Two capacitors C_{in3} and C_{in4} having the same value are used to reduce the gain at low frequencies and function as dc block capacitors. The dual-band input matching network consists of capacitor C_5 having the same value with C_{in3} and C_{in4}, Network 9 consisting of L_1, C_1, L_2, and C_2, and Network 1 consisting of L_3 and C_3.

1) L_1, C_1, L_2, and C_2 (Network 9): Network 9 consisting of L_1, C_1, L_2, and C_2 is used to synthesize the inductor L_{in1} at $f_1 = 25.5$ GHz and C_{in1} at $f_2 = 37$ GHz, while acting as short-circuit at 18 and 51 GHz to reject the out-of-band signals and shape the dual-band gain response. Values for C_{11}, L_{11}, C_{12}, and L_{12} are obtained by solving (1) and (2) with the use of Network 9's impedance expression and short-circuit condition, resulting in $C_1 = 457$ fF, $L_1 = 171$ pH, $C_2 = 130$ fF, and $L_2 = 75$ pH.

2) L_3 and C_3 (Network 1): Network 1 consisting of L_3 and C_3 is used to synthesize the capacitor C_{in2} at 25.5 GHz and
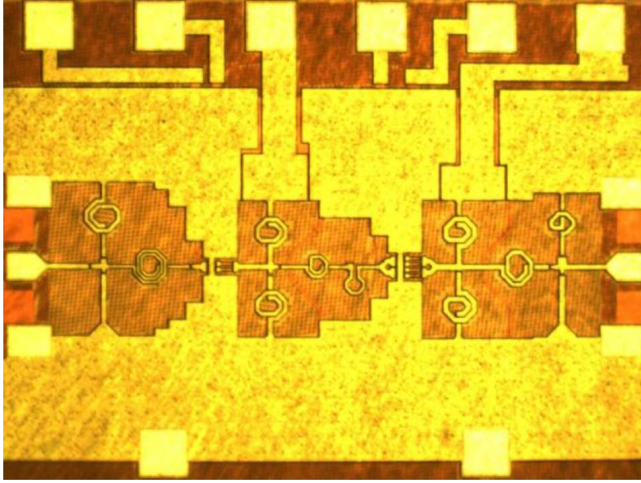
Fig. 8. Microphotograph of the 25.5/37-GHz dual-band PA.

Fig. 9. Measured and simulated small-signal S-parameters.

inductor L_{in2} at 37 GHz. The capacitor C_3 also functions as a dc block capacitor preventing dc current from the base of transistor Q1 feeding through the 50-Ω source. L_3 and C_3 are obtained from (1) and (2) as $L_{10} = 316$ pH and $C_{10} = 85$ fF.

F. PA Layout and Fabrication

The 25.5/37-GHz concurrent dual-band PA was laid-out using Cadence. In the layout, the inductors are placed sufficiently far away from each other to reduce the inter-coupling while minimizing the chip area. All inductors in each dual-band matching network are simulated as a whole using IE3D to verify the performance after individual inductors have been laid out. Fig. 8 shows a microphotograph of the dual-band PA. It has a chip area of 1.3×0.68 mm^2.

IV. DUAL-BAND PA PERFORMANCE

The designed concurrent dual-band PA was measured on-chip using a Rhode & Schwarz vector network analyzer and Cascade probe station. The short–open–load–thru calibration method along with Microtech's impedance standard substrate standards was used. The unconditional stability of the PA was confirmed through simulated and measured results.

In concurrent multiband components, both single- and multimode operation can occur. Single-mode operation occurs when there exist only signals in one band, while multimode operation happens when signals in multiple bands occur at the same time. Multi-mode operation is especially important for concurrent multi-band components since it truly characterizes the performance of these components.

Fig. 9 shows the simulated and measured S-parameters of the concurrent dual-band PA under small-signal conditions. The dual-band PA exhibits gains ($S21$) of 21.4 dB and 17 dB, 3-dB bandwidths of 3.7 and 1.8 GHz, input return losses ($S11$) of 14.8 and 9 dB, and output return losses ($S22$) of 12.5 and 15 dB at 25.5 and 37 GHz, respectively. The reverse isolation ($S12$) is higher than 35 dB from dc to 55 GHz. The PA has a good dual-band gain response with out-of-band rejection below 0 dB from dc to 20, 30.5 to 34, and above 43 GHz. The rejection of signals at 32.5 GHz is 15 dB, while that at frequencies below 10 GHz and above 50 GHz is larger than 30 dB, resulting in
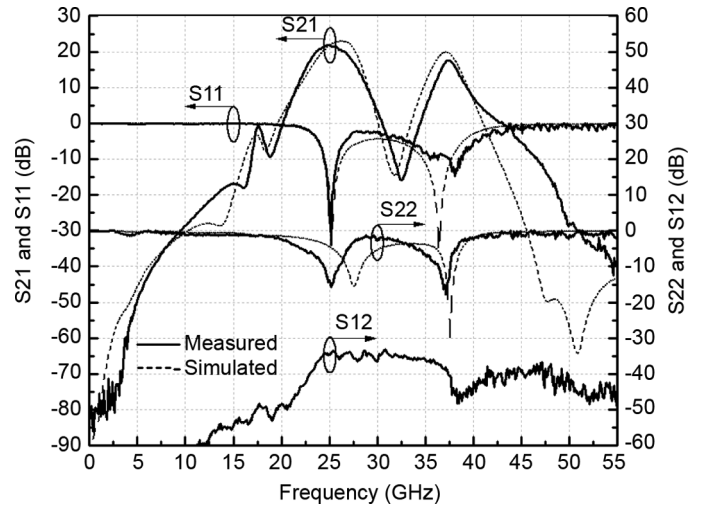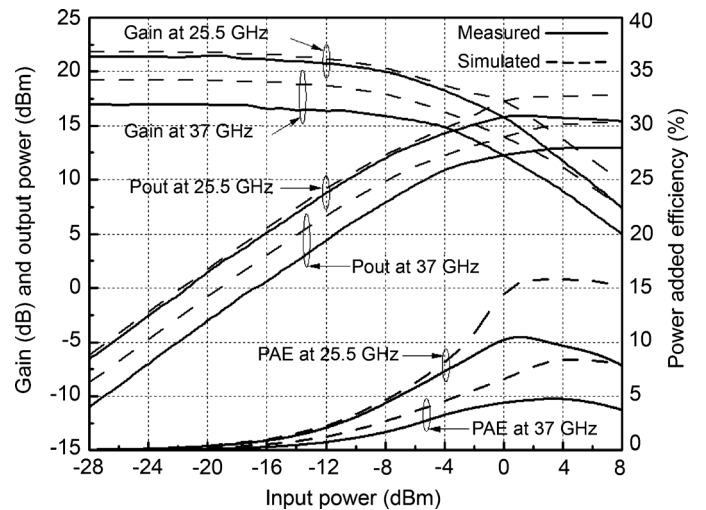

Fig. 10. Measured and simulated gain, output power, and PAE at 25.5 and 37 GHz in single-band mode.

good suppression of the harmonics, IMPs, and out-of-band signals, which are important for dual-band PA design. These characteristics are indeed achieved from the concurrent dual-band synthetic matching technique implemented for the input, interstage, and output matching networks, as expected. The PA consumes a current of 120 mA from a 3-V supply voltage.

The simulated and measured results are in good agreement from dc to 41 GHz. Particularly, the peak-gain differences between the measured and simulated results at 25.5 and 37 GHz are 0.6 and 2.6 dB, respectively. These discrepancies are primarily due to the inaccuracy of the active and passive device models at millimeter-wave frequencies, which are inevitable for RFICs operating in the millimeter-wave regime. For comparison purposes, we also simulated the performances of the single-band PAs. The simulation results show that the designed concurrent dual-band PA has 1.8- and 2.5-dB smaller gain than the corresponding single-band PAs at 25.5 and 37 GHz, respectively. The series ($L_4 - C_4$) and shunt ($L_7 - C_7$) resonators help shape the dual-band gain through their resonant frequencies at 32.5 GHz. It is noted that most of the LC networks used in the
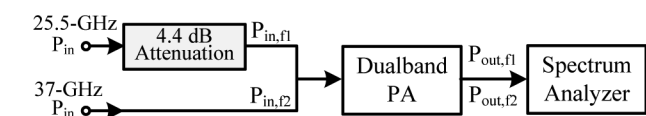
Fig. 11. Simplified test bench for the PA measurement in the dual-band mode.
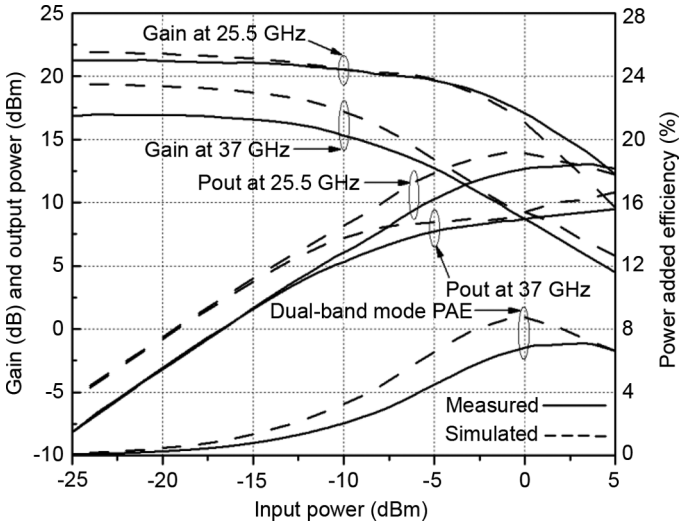

Fig. 12. Measured and simulated gain, output power, and PAE in the 25.5/37-GHz dual-band mode.
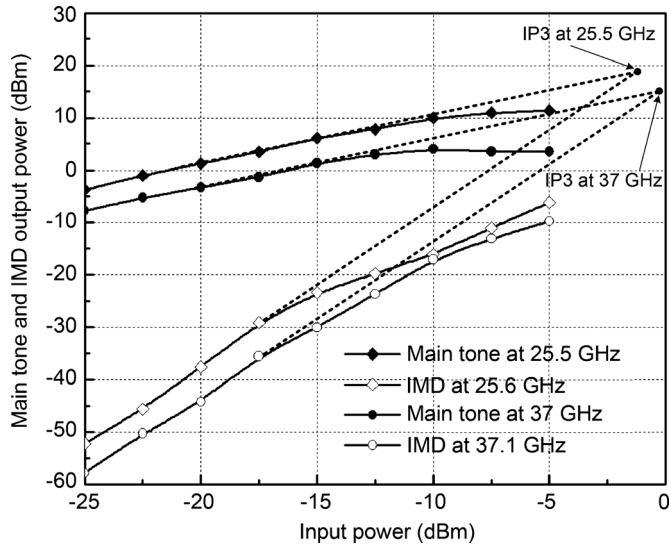

Fig. 13. Two-tone measurement for each band of the dual-band PA.

TABLE I
SUMMARY OF THE PA PERFORMANCE IN SINGLE- AND DUAL-BAND MODE

Parameter	Single-band mode				Dual-band mode			
	Simulated		Measured		Simulated		Measured	
Freq (GHz)	25.5	37	25.5	37	25.5	37	25.5	37
Gain (dB)	22	19.6	21.4	17	22	19.6	21.4	17
Input RL (dB)	21.3	17.1	14.8	9.1	21.3	17.1	14.8	9.1
Output RL (dB)	5.4	10.2	12.5	15	5.4	10.2	12.5	15
$P_{out,max}$ (dBm)	17.8	15.4	16	13	14	11	13	9.5
$P_{out,1dB}$ (dBm)	10.8	8.8	10.4	7.1	6.5	5.4	6.8	4.6
PAE_{max} (%)	15.8	8.4	10.6	4.9	8.8		7.1	
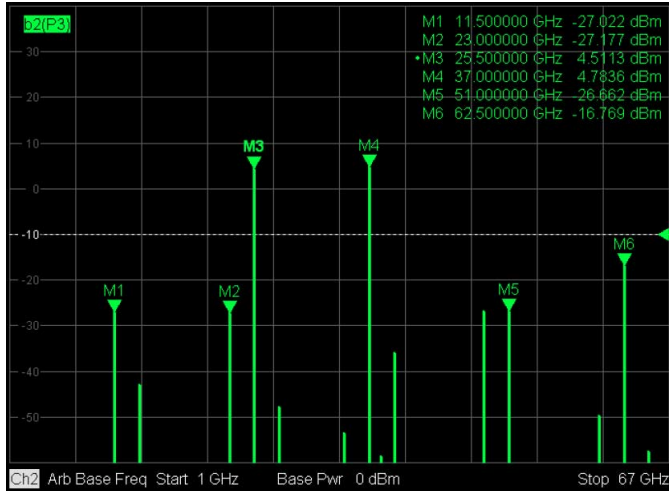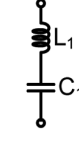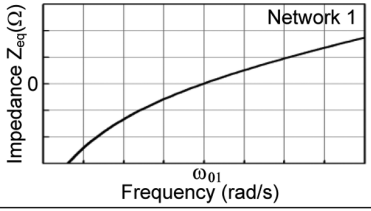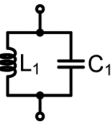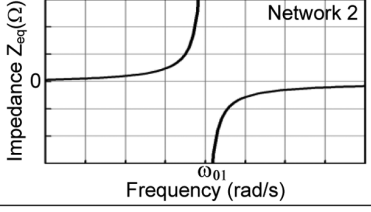
Fig. 14. Measured output spectrum of the dual-band PA in the dual-band mode in the saturated operation.
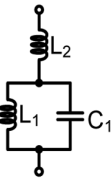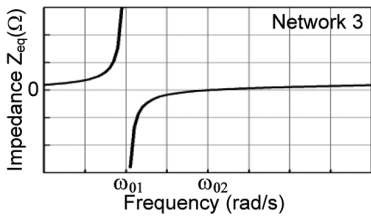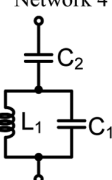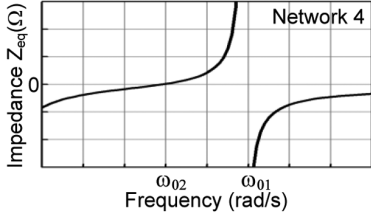
TABLE II
COMPARISON OF Si-BASED PAs IN K- AND Ka-BANDS

Ref.	Process	Freq (GHz)	$P_{out,max}$ (dBm)	$P_{out,1dB}$ (dBm)	PAE (%)	Gain (dB)	Supply (V)	Oper-ation
[15]	0.2μm SiGe	21-26	20-23	18.8	10-19.7	15-19	1.8	Single-band
[16]	0.5μm SiGe	24	12	11	2.9	18	5	Single-band
[17]	0.5μm SiGe	24	-	12	2.7	17.7	3	Single-band
[18]	0.18μm SiGe	24	22	20	14	12	5	Single-band
[19]	0.18μm CMOS	24	14.5	12	6.5	7	2.8	Single-band
[17]	0.5μm SiGe	36	-	10	1.5	15.3	3	Single-band
This work	0.18μm SiGe	25.5	16	10.4	10.6	21.4	3	Dual-band (Single-mode)
This work	0.18μm SiGe	37	13	7.1	4.9	17	3	Dual-band (Single-mode)

dual-band PA change their equivalent impedance from inductance to capacitance, or vice versa, when the frequency crosses this notch point.

Fig. 10 shows the measured and simulated gain, output power and the PAE in the single-band mode at 25.5 and 37 GHz. The measured results show that, in the single-band mode, the maximum output powers, $P_{out,max}$, reach 16 and 13 dBm, output 1-dB compression points, $P_{out,1dB}$, are 10.4 and 7.1 dBm, and maximum PAEs, PAE_{max}, are 10.6 and 4.9% at 25.5 and 37 GHz, respectively.

Since the PA gain at 25.5 GHz is higher than that at 37 GHz, as seen in Fig. 10, the output power at 25.5 GHz is always

higher than that at 37 GHz for the same input power. Therefore, in the dual-band mode and under equal input power, the 25.5-GHz signal would desensitize the 37-GHz signal, so that

TABLE A1
LC NETWORKS AND THEIR IMPEDANCES/ADMITTANCES, CHARACTERISTICS, AND IMPEDANCE PLOTS

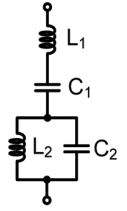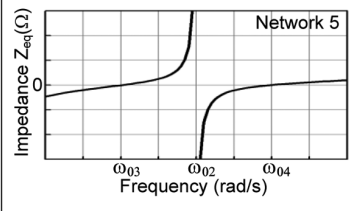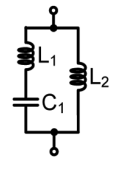| LC Network	Impedance/Admittance	Characteristic	Impedance plot
Network 1 (L_1 and C_1 in series)	$Z_{eq}=j(\omega L_1-\frac{1}{\omega C_1})$ $=\frac{j(\omega^2-\omega_{01}^2)}{\omega\omega_{01}^2 C_1}$ $\omega_{01}=\frac{1}{\sqrt{L_1 C_1}}$	$Z_{eq}=0$ at $\omega=\omega_{01}$ $L_{eq}=\frac{\omega^2-\omega_{01}^2}{\omega^2\omega_{01}^2 C_1}$ at $\omega>\omega_{01}$ $C_{eq}=\frac{\omega_{01}^2 C_1}{\omega_{01}^2-\omega^2}$ at $\omega<\omega_{01}$	
Network 2 (L_1 parallel C_1)	$Z_{eq}=\frac{j\omega\omega_{01}^2 L_1}{(\omega_{01}^2-\omega^2)}$ $\omega_{01}=\frac{1}{\sqrt{L_1 C_1}}$	$Z_{eq}=\infty$ at $\omega=\omega_{01}$ $L_{eq}=\frac{\omega_{01}^2 L_1}{\omega_{01}^2-\omega^2}$ at $\omega<\omega_{01}$ $C_{eq}=\frac{\omega^2-\omega_{01}^2}{\omega^2\omega_{01}^2 L_1}$ at $\omega>\omega_{01}$	
Network 3 (L_2 series with $L_1 \parallel C_1$)	$Z_{eq}=j\omega L_2+\frac{j\omega\omega_{01}^2 L_1}{(\omega_{01}^2-\omega^2)}$ $\omega_{01}=\frac{1}{\sqrt{L_1 C_1}}$ $\omega_{02}=\omega_{01}\sqrt{\frac{L_1+L_2}{L_2}}$	$Z_{eq}=\infty$ at $\omega=\omega_{01}$ $Z_{eq}=0$ at $\omega=\omega_{02}$ $L_{eq}=L_2+\frac{\omega_{01}^2 L_1}{\omega_{01}^2-\omega^2}$ at $\omega<\omega_{01}$ or $\omega>\omega_{02}$ $C_{eq}=\left(-\omega^2 L_2+\frac{\omega^2\omega_{01}^2 L_1}{\omega^2-\omega_{01}^2}\right)^{-1}$ at $\omega_{01}<\omega<\omega_{02}$	
Network 4 (C_2 series with $L_1 \parallel C_1$)	$Z_{eq}=\frac{1}{j\omega C_2}+\frac{j\omega\omega_{01}^2 L_1}{\omega_{01}^2-\omega^2}$ $\omega_{01}=\frac{1}{\sqrt{L_1 C_1}}$ $\omega_{02}=\omega_{01}\sqrt{\frac{C_2}{C_1+C_2}}$	$Z_{eq}=\infty$ at $\omega=\omega_{01}$ $Z_{eq}=0$ at $\omega=\omega_{02}$ $L_{eq}=\frac{-1}{\omega^2 C_2}+\frac{\omega_{01}^2 L_1}{\omega_{01}^2-\omega^2}$ at $\omega_{02}<\omega<\omega_{01}$ $C_{eq}=\left(\frac{1}{C_2}+\frac{\omega^2\omega_{01}^2 L_1}{\omega^2-\omega_{01}^2}\right)^{-1}$ at $\omega<\omega_{02}$ or $\omega>\omega_{01}$	
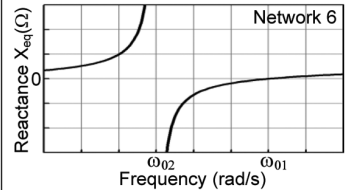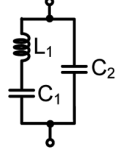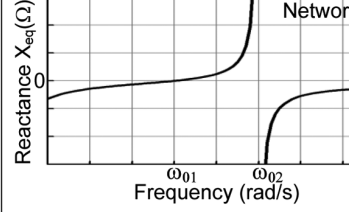
the PA reaches a saturation state with much larger output power at 25.5 GHz than 37 GHz. In order to increase the 37-GHz saturation power, the input power at 25.5 GHz would need to be lower than that at 37 GHz.

Fig. 11 shows a simplified test bench for the PA measurement in the dual-band mode, in which two continuous wave (CW) signals at 25.5 and 37 GHz are applied to the PA simultaneously. P_{in} is the initial (equal) input power of each tone, and $P_{in,f1} = P_{in} - 4.4$ dBm and $P_{in,f2} = P_{in}$ are the input powers (in dBm) at 25.5 and 37 GHz, respectively. The input power of the 25.5-GHz tone is set to be 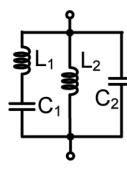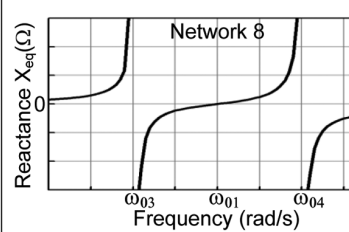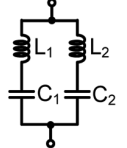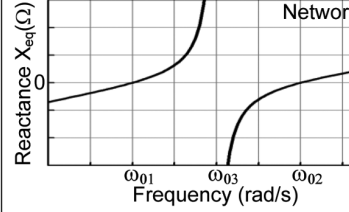4.4 dB lower than that of the 37-GHz tone to ensure that the PA gives the same output power at both frequencies under small input-signal conditions, making use of the result that the difference of the two measured small-signal gains at 25.5 and 37 GHz is 4.4 dB, as seen in Fig. 9. The same test bench is also used in the simulation using a 2.4-dB difference between the input powers at 25.5 and 37 GHz, which is the difference of the two simulated gains at these frequencies, as shown in Fig. 9.

Fig. 12 shows the measured and simulated gain, output power, and PAE in the dual-band mode. It is noted that the input power in the x-axis of Fig. 12 is P_{in}, which is also equal to the input power of the 37-GHz tone $(P_{in,f2})$ in Fig. 11. As shown in Fig. 12, the measured output power of the 25.5- and 37-GHz signals are the same until their input power P_{in} reaches -12.5 dBm. After that point, the 37-GHz output power is gradually saturated while the 25.5-GHz output power keeps increasing for several dBm until it saturates. This shows different nonlinear behaviors of the active devices and the PA at large-signal conditions, and the linearity of the PA at 25.5 GHz is higher than that at 37 GHz. The results in Fig. 12 signify that the nonlinearity of the PA is different for different frequencies, as well as for dual and single mode. The measured results also show that, in the dual-band mode, the maximum output powers are 13 and 9.5 dBm, and the output 1-dB compression powers are 6.8 and 4.6 dBm at 25.5 and 37 GHz, respectively. It is observed that in the dual-band mode, the 25.5- and 37-GHz signals become compressed at input power several dBm lower than that in the single-band mode, and the maximum and 1-dB compression output power in the dual-band mode are lower than those in the single-band mode.

TABLE A1 *(Continued.)*
LC NETWORKS AND THEIR IMPEDANCES/ADMITTANCES, CHARACTERISTICS AND IMPEDANCE PLOTS

Network 5	$Z_{eq} = \dfrac{j(\omega^2 - \omega_{01}^2)}{\omega\omega_{01}^2 C_1} + \dfrac{j\omega\omega_{02}^2 L_2}{\omega_{02}^2 - \omega^2}$ $\omega_{01} = \dfrac{1}{\sqrt{L_1 C_1}},\ \omega_{02} = \dfrac{1}{\sqrt{L_2 C_2}}$ $\omega_{03} = \sqrt{B - \dfrac{\sqrt{B^2 - 4C}}{2}}$ $\omega_{04} = \sqrt{B + \dfrac{\sqrt{B^2 - 4C}}{2}}$ $B = \omega_{01}^2 + \omega_{02}^2 + \omega_{01}^2\omega_{02}^2 L_2 C_1$ $C = \omega_{01}^2 \omega_{02}^2$	$Z_{eq} = \infty$ at $\omega = \omega_{02}$ $Z_{eq} = 0$ at $\omega = \omega_{03}, \omega_{04}$ $L_{eq} = \dfrac{\omega^2 - \omega_{01}^2}{\omega^2\omega_{01}^2 C_1} + \dfrac{\omega_{02}^2 L_2}{\omega_{02}^2 - \omega^2}$ at $\omega_{03} < \omega < \omega_{02}$ or $\omega > \omega_{04}$ $C_{eq} = \left(\dfrac{\omega_{01}^2 - \omega^2}{\omega_{01}^2 C_1} + \dfrac{\omega^2\omega_{02}^2 L_2}{\omega^2 - \omega_{02}^2} \right)^{-1}$ at $\omega < \omega_{03}$ or $\omega_{02} < \omega < \omega_{04}$	
Network 6	$Y_{eq} = \dfrac{j\omega\omega_{01}^2 C_1}{\omega_{01}^2 - \omega^2} + \dfrac{1}{j\omega L_2}$ $X_{eq} = (Y_{eq})^{-1}$ $\omega_{01} = \dfrac{1}{\sqrt{L_1 C_1}}$ $\omega_{02} = \omega_{01}\sqrt{\dfrac{L_1}{L_1 + L_2}}$	$X_{eq} = 0$ at $\omega = \omega_{01}$ $X_{eq} = \infty$ at $\omega = \omega_{02}$ $L_{eq} = \left(\dfrac{\omega^2\omega_{01}^2 C_1}{\omega^2 - \omega_{01}^2} + \dfrac{1}{L_2} \right)^{-1}$ at $\omega < \omega_{02}$ or $\omega > \omega_{01}$ $C_{eq} = \dfrac{\omega_{01}^2 C_1}{\omega_{01}^2 - \omega^2} - \dfrac{1}{\omega^2 L_2}$ at $\omega_{02} < \omega < \omega_{01}$	
Network 7	$Y_{eq} = \dfrac{j\omega\omega_{01}^2 C_1}{\omega_{01}^2 - \omega^2} + j\omega C_2$ $X_{eq} = (Y_{eq})^{-1}$ $\omega_{01} = \dfrac{1}{\sqrt{L_1 C_1}}$ $\omega_{02} = \omega_{01}\sqrt{\dfrac{C_1 + C_2}{C_2}}$	$X_{eq} = 0$ at $\omega = \omega_{01}$ $X_{eq} = \infty$ at $\omega = \omega_{02}$ $L_{eq} = \left(\dfrac{\omega^2\omega_{01}^2 C_1}{\omega^2 - \omega_{01}^2} - \omega^2 C_2 \right)^{-1}$ at $\omega_{01} < \omega < \omega_{02}$ $C_{eq} = \dfrac{\omega_{01}^2 C_1}{\omega_{01}^2 - \omega^2} + C_2$ at $\omega < \omega_{01}$ or $\omega > \omega_{02}$	
Network 8	$Y_{eq} = \dfrac{j\omega\omega_{01}^2 C_1}{\omega_{01}^2 - \omega^2} + \dfrac{\omega_{02}^2 - \omega^2}{j\omega\omega_{02}^2 L_2}$ $X_{eq} = (Y_{eq})^{-1}$ $\omega_{01} = \dfrac{1}{\sqrt{L_1 C_1}},\ \omega_{02} = \dfrac{1}{\sqrt{L_2 C_2}}$ $\omega_{03} = \sqrt{B - \dfrac{\sqrt{B^2 - 4C}}{2}}$ $\omega_{04} = \sqrt{B + \dfrac{\sqrt{B^2 - 4C}}{2}}$ $B = \omega_{01}^2 + \omega_{02}^2 + \omega_{01}^2\omega_{02}^2 L_2 C_1$ $C = \omega_{01}^2 \omega_{02}^2$	$X_{eq} = 0$ at $\omega = \omega_{01}$ $X_{eq} = \infty$ at $\omega = \omega_{03}, \omega_{04}$ $L_{eq} = \left(\dfrac{\omega^2\omega_{01}^2 C_1}{\omega^2 - \omega_{01}^2} + \dfrac{\omega^2 - \omega_{02}^2}{\omega_{02}^2 L_2} \right)^{-1}$ at $\omega < \omega_{03}$ or $\omega_{01} < \omega < \omega_{04}$ $C_{eq} = \dfrac{\omega_{01}^2 C_1}{\omega_{01}^2 - \omega^2} + \dfrac{\omega^2 - \omega_{02}^2}{\omega^2\omega_{02}^2 L_2}$ at $\omega_{03} < \omega < \omega_{01}$ or $\omega > \omega_{04}$	
Network 9	$Y_{eq} = \dfrac{j\omega\omega_{01}^2 C_1}{\omega_{01}^2 - \omega^2} + \dfrac{j\omega\omega_{02}^2 C_2}{\omega_{02}^2 - \omega^2}$ $X_{eq} = (Y_{eq})^{-1}$ $\omega_{01} = \dfrac{1}{\sqrt{L_1 C_1}},$ $\omega_{02} = \dfrac{1}{\sqrt{L_2 C_2}}$ $\omega_{03} = \omega_{01}\omega_{02}\sqrt{\dfrac{C_1 + C_2}{\omega_{01}^2 C_1 + \omega_{02}^2 C_2}}$	$X_{eq} = 0$ at $\omega = \omega_{01}, \omega_{02}$ $X_{eq} = \infty$ at $\omega = \omega_{03}$ $L_{eq} = \left(\dfrac{\omega^2\omega_{01}^2 C_1}{\omega^2 - \omega_{01}^2} + \dfrac{\omega^2\omega_{02}^2 C_2}{\omega^2 - \omega_{02}^2} \right)^{-1}$ at $\omega_{01} < \omega < \omega_{03}$ or $\omega > \omega_{02}$ $C_{eq} = \dfrac{\omega_{01}^2 C_1}{\omega_{01}^2 - \omega^2} + \dfrac{\omega_{02}^2 C_2}{\omega_{02}^2 - \omega^2}$ at $\omega < \omega_{01}$ or $\omega_{03} < \omega < \omega_{02}$	

It is noted that the PAE in the dual-band mode is expected to be different from that for the single-band mode. In order to take into account the effects of concurrent dual-band operation for PA, we define the PAE for the dual-band mode as

$$\text{PAE} = \frac{P_{\text{out},f1} + P_{\text{out},f2} - (P_{\text{in},f1} + P_{\text{in},f2})}{P_{\text{DC}}} \quad (13)$$

where $P_{\text{out},f1}$ and $P_{\text{out},f2}$ are the output powers of the PA at 25.5 and 37 GHz, respectively, as indicated in Fig. 11. P_{DC} is the dc power. The measured results show that the maximum dual-band-mode PAE is 7.1%.

Two-tone test was performed to characterize the nonlinearity of the dual-band PA in each band. Two-tone signals

of 25.5/25.55 and 37/37.05 GHz were used to measure the output-referred third-order intercept point (OIP3) in the 25.5- and 37-GHz bands, respectively. The measured output powers of the main tones at 25.5 and 37 GHz, and the intermodulation distortion (IMD) products at 25.6 and 37.1 GHz are shown in Fig. 13. These results show that the OIP3 is 18.5 and 15 dBm in the 25.5- and 37-GHz bands, respectively.

Table I summarizes the performance of the designed concurrent dual-band PA in the single- and dual-band mode. The maximum difference between the simulated and measured results of gain, $P_{\text{out,max}}$, $P_{\text{out,1 dB}}$, and PAE_{max} are 2.6 dB, 2.4 dBm, and 1.7 dBm and 5.2% in the single-band mode, and 2.6 dB, 3.5 dBm, and 2.2 dBm, and 1.7% in the dual-band mode, respectively. The input and output return losses were measured in the single-band mode under a small-signal condition and used for the dual-band mode. These measured single- and dual-band mode return losses are expected to be the same under small-signal conditions since the PA operation was linear and there was no significant interaction between the signals of the two bands.

Fig. 14 displays the screen capture from the VNA showing the output spectrum of the designed PA in the dual-band mode. In this measurement, the two fundamental tones at 25.5 and 37 GHz were used simultaneously as the input to the PA. The input power levels of the two tones were increased to drive the PA into saturation and the output powers of the two tones roughly 9 dBm. About 4.5 dB is added to the observed power levels on the spectrum display to compensate for the cable, connector, and RF probe losses. It is observed that all the IMP and harmonic powers are at least 30 dB lower than those of the two main tones, except the IMP power at 62.5 GHz, which is 21 dB lower. These results demonstrate good harmonic/IMP suppression of the designed PA, which results from the proposed dual-band matching filtering technique. Table II compares the performance of the designed dual-band PA operating in single-band modes to those of recently reported silicon-based fully integrated single-band PAs. It is particularly noted that the designed PA is intended for concurrent dual-band operation, not for single-band usage, and hence, its comparison to other single-band PAs, while provided for reference purposes, does not really have an effective implication. As stated earlier, there has been no concurrent dual-band PA operating above 5.2 GHz reported.

V. CONCLUSION

A new concurrent dual-band impedance-matching filtering methodology has been presented together with a 25.5/37-GHz concurrent dual-band PA. The proposed technique facilitates the design of various concurrent dual-band matching networks, each being synthesized from two single-band matching networks. The resultant dual-band matching filtering networks can be used to achieve not only concurrent matching between two arbitrary loads and two arbitrary sources at any dual-band frequencies, but also suppression of unwanted signals like the harmonics and IMPs. They are especially attractive for on-chip realization for RFICs. Various other dual-band matching filtering networks using lumped elements, transmission lines, or their combination can be developed based on the proposed

method. The presented dual-band matching filtering technique can also be implemented to derive concurrent multi-band matching filtering networks having more than two bands. The designed concurrent dual-band PA produces good performance for both single and dual modes at 25.5 and 37 GHz with good dual-band shaped gain, and good capability of harmonic/IMP suppression resulting in improved linearity. The concurrent dual-band matching filtering technique, through its successful implementation for a concurrent dual-band PA design, implicitly demonstrates that multi-band components, such as PAs, low-noise amplifiers, mixers, etc., can be designed relatively easy, facilitating the design of modern multiband/multimode communication and radar systems that have many benefits.

APPENDIX

Table A1 shows nine LC networks together with their impedance/admittance expressions, characteristics, and impedance plots, where L_{eq}, C_{eq}, Z_{eq}, and Y_{eq} are the equivalent inductance, capacitance, impedance, and admittance of the networks, respectively, and $\omega_{0i}(i = 1, 2, \ldots, 4)$ are the frequencies at which the networks become a short or open. More complicated LC networks and their characteristics can easily be derived from those in Table A1. Networks 1 and 2 are the same as those used in [7]. These LC networks are not dual band. However, they can be used in the proposed concurrent dual-band matching filtering design technique described in Section II to synthesize dual-band matching filtering networks.

REFERENCES

[1] S. Zhang, J. Madic, P. Bretchko, J. Mokoro, R. Shumovich, and R. McMorrow, "A novel power-amplifier module for quad-band wireless handset applications," *IEEE Trans. Microw. Theory Techn.*, vol. 51, no. 11, pp. 2203–2210, Nov. 2003.

[2] K. Yamamoto, S. Suzuki, K. Mori, T. Asada, T. Okuda, A. Inoue, T. Miura, K. Chomei, R. Hattori, M. Yamanouchi, and T. Shimura, "A 3.2-V operation single-chip dual-band AlGaAs/GaAs HBT MMIC power amplifier with active feedback circuit technique," *IEEE J. Solid-State Circuits*, vol. 35, no. 8, pp. 1109–1120, Aug. 2000.

[3] H. Zhang, H. Gao, and G. P. Li, "Broad-band power amplifier with a novel tunable output matching network," *IEEE Trans. Microw. Theory Techn.*, vol. 53, no. 11, pp. 3606–3614, Nov. 2005.

[4] L. Yumin, D. Peroulis, S. Mohammadi, and L. P. B. Katehi, "A MEMS reconfigurable matching network for a class AB amplifier," *IEEE Microw. Wireless Compon. Lett.*, vol. 13, no. 10, pp. 437–439, Oct. 2003.

[5] W. C. E. Neo, Y. Lin, X. D. Liu, L. C. N. D. Vreede, L. E. Larson, M. Spirito, M. J. Pelk, K. Buisman, A. Akhnoukh, A. D. Graauw, and L. K. Nanver, "Adaptive multi-band multi-mode power amplifier using integrated varactor-based tunable matching networks," *IEEE J. Solid-State Circuits*, vol. 41, no. 9, pp. 2166–2176, Sep. 2006.

[6] M. R. Ghajar and S. Boumaiza, "Concurrent dual band 2.4/3.5 GHz fully integrated power amplifier in 0.13 μm CMOS technology," in *Proc. Eur. Microw. Conf.*, Rome, Italy, Sep. 2009, pp. 375–378.

[7] S.-F. R. Chang, W. L. Chen, S. C. Chang, C. K. Tu, C. L. Wei, C. H. Chien, C. H. Tsai, J. Chen, and A. Chen, "A dual-band RF transceiver for multistandard WLAN applications," *IEEE Trans. Microw. Theory Techn.*, vol. 53, no. 3, pp. 1048–1055, Mar. 2005.

[8] P. Colantonio, F. Giannini, R. Giofre, and L. Piazzon, "A design technique for concurrent dual-band harmonic tuned power amplifier," *IEEE Trans. Microw. Theory Techn.*, vol. 56, no. 11, pp. 2545–2555, Nov. 2008.

[9] W. Chen, S. A. Bassam, Li Xiang, Y. Liu, K. Rawat, M. Helaoui, F. M. Ghannouchi, and Z. Feng, "Design and linearization of concurrent dual-band Doherty power amplifier with frequency-dependent power ranges," *IEEE Trans. Microw. Theory Techn.*, vol. 59, no. 10, pp. 2537–2545, Oct. 2011.

[10] Y. Wu, Y. Liu, Li Shulan, C. Yu, and X. Liu, "A generalized dual-frequency transformer for two arbitrary complex frequency-dependent impedances," *IEEE Microw. Wireless Compon. Lett.*, vol. 19, no. 12, pp. 792–794, Dec. 2009.

[11] M.-L. Chuang, "Dual-band impedance transformer using two section shunt stub," *IEEE Trans. Microw. Theory Techn.*, vol. 58, no. 5, pp. 1257–1263, May 2010.

[12] K.-A. Hsieh, H.-S. Wu, K.-H. Tsai, and C.-K. Tzuang, "A dual-band 10/24-GHz amplifier design incorporating dual-frequency complex load matching," *IEEE Trans. Microw. Theory Techn.*, vol. 60, no. 6, pp. 1649–1657, Jun. 2012.

[13] K. Rawat and F. M. Ghannouchi, "Dual-band matching technique based on dual-characteristic impedance transformers for dual-band power amplifiers design," *IET Microw., Antennas, Propag.*, vol. 5, no. 14, pp. 1720–1729, 2011.

[14] R. J. Trew, "High-frequency solid-state electronic devices," *IEEE Trans. Electron Devices*, vol. 52, no. 5, pp. 638–648, May 2005.

[15] T. S. D. Cheung and J. R. Long, "A 21–26-GHz sige bipolar power amplifier MMIC," *IEEE J. Solid-State Circuits*, vol. 40, no. 12, pp. 2583–2597, Dec. 2005.

[16] N. Kinayman, A. Jenkins, D. Helms, and I. Gresham, "Design of 24 GHz SiGe HBT balanced power amplifier for system-on-a-chip ultra-wideband applications," in *IEEE RFIC Symp. Dig.*, Jun. 2005, pp. 91–94.

[17] S. Chartier, E. Sonmez, and H. Schumacher, "24 and 36 GHz SiGe HBT power amplifiers," *Silicon Monolithic Integr. Circuits in RF Syst. Dig.*, pp. 251–254, Sep. 2004.

[18] J. P. Comeau, J. M. Andrews, and J. D. Cressler, "A monolithic 24 GHz, 20 dBm, 14% PAE SiGe HBT power amplifier," in *Proc. Eur. Microw. Conf.*, Sep. 2006, pp. 419–422.

[19] A. Komijani, A. Natarajan, and A. Hajimiri, "A 24-GHz, +14.5-dBm fully integrated power amplifier in 0.18-μm CMOS," *IEEE J. Solid-State Circuits*, vol. 40, no. 9, pp. 1901–1908, Sep. 2005.

[20] G. Gonzalez, *Microwave Transistor Amplifiers Analysis and Design*, 2nd ed ed. Englewood Cliffs, NJ, USA: Prentice-Hall, 1997.

[21] A. N. Stameroff, A. Pham, and R. E. Leoni, "High efficiency push–pull inverse class F power amplifier using a balun and harmonic trap waveform shaping network," in *IEEE MTT-S Int. Microw. Symp. Dig.*, May 2010, pp. 521–525.

[22] C. M. Grens, P. Cheng, and J. D. Cressler, "Reliability of SiGe HBTs for power amplifiers—Part I: Large-signal RF performance and operating limits," *IEEE Trans. Device Mater. Rel.*, vol. 9, no. 3, pp. 431–439, Sep. 2009.

[23] M. Rickelt, H.-M. Rein, and E. Rose, "Influence of impact-ionization-induced instabilities on the maximum usable output voltage of Si-bipolar transistors," *IEEE Trans. Electron Devices*, vol. 48, no. 4, pp. 774–783, Apr. 2001.

Cuong Huynh (S'08–M'11) received the B.S. and M.S. degrees in electrical engineering from Ho Chi Minh University of Technology (HCMUT), Ho Chi Minh City, Vietnam, in 1998 and 2003, respectively, and the Ph.D. degree in electrical engineering from Texas A&M University, College Station, TX, USA, in 2012.

From 2006 to 2012, he was a Research Assistant with the Sensing, Imaging and Communication Systems Laboratory, Texas A&M University, where he conducted research on multi-band RFIC transceivers for wireless communication and radar systems. From 2011 to 2012, he was an Intern with the Mobile and Wireless Group, Broadcom Inc., Irvine, CA, USA. He is currently an Assistant Professor of electrical engineering with HCMUT. His current research interests include microwave and millimeter-wave RFICs.

Cam Nguyen (S'82–M'83–SM'91–F'05) joined the Department of Electrical and Computer Engineering, Texas A&M University, in December 1990, where he is currently the Texas Instruments Endowed Professor, after working for over 12 years in industry. From 2003 to 2004, he was Program Director with the National Science Foundation (NSF), where he was responsible for research programs in RF electronics and wireless technologies. While in industry, he led numerous microwave and millimeter-wave activities and developed many microwave and millimeter-wave integrated circuits and systems up to 220 GHz. His research group at Texas A&M University currently focuses on Si RFICs and systems for wireless communications, radar, and sensing. He is the founding Editor-in-Chief of *Sensing and Imaging: An International Journal* (a Springer publication).